CHEMICAL ENGINEERING TRANSACTIONS
VOL. 66, 2018
A publication of AIDIC
The Italian Association of Chemical Engineering
Online at www.aidic.it/cet
Guest Editors: Songying Zhao, Yougang Sun, Ye Zhou

ISBN 978-88-95608-63-1; **ISSN** 2283-9216
DOI: 10.3303/CET1866187

Numerical Seismic Performance Model of Frame-Supported Shear Wall with Carbon Fibre Reinforced Plastic Bars in Transfer Beam based on OpenSees

Weilai Yao*, Shiyong Jiang, Shuai Tao, Shijuan Wu

Department of Military Infrastructure Engineering, Army Logistics University of PLA, Chongqing 401311, China
futureYWL@hotmail.com

This paper studies the seismic behaviours of frame-support shear wall under cyclic loading. Two specimens were created for detailed analysis. One of the specimen was a frame-support shear wall reinforced by carbon fibre reinforced plastic (CFRP) bars, and the other by steel bars. Based on an experimental study of three frame-support shear walls, the finite-element analysis software OpenSees was adopted to conduct further theoretical research. Based on the fibre beam column model, the Pinching4 material and zero-length rotational spring were applied, and a numerical analysis model was established to analyse the walls, considering the bond slip of longitudinal reinforcement. It was shown that the numerical model considering the bond slip properly simulated the hysteresis curves of the specimens under cyclic loading, including the pinch effect. The model also achieved a good accuracy in the simulation of the yield load and ultimate load.

1. Introduction

In recent years, fibre reinforced plastic (FRP) has become a hot topic in the field of civil engineering thanks to its high strength and corrosion resistance. Because of the poor crack resistance of concrete, steel bars are easily corroded when reinforced concrete structures are exposed to erosion. To ensure the safety and durability of the structures, one of the most common practices is to replace the steel bars with FRP bars, especially the carbon fibre reinforced plastic (CFRP) bars. For instance, the steel bar corrosion can be effectively resolved by adopting the CFRP bars for frame-supported shear walls. However, the CFRP, as a linear elastic material with no yield step, may suffer from brittle failure and affect the seismic performance of the structure (Grace et al., 2005; Dong et al., 2013; Whitehead, 2005; Ge et al., 2011; Micelli et al., 2014). There have been extensive discussions on the seismic performance of frame-supported shear wall with steel bars at home and abroad (Liang and Cai, 2011), but relatively few experimental studies on frame-supported shear wall with CFRP bars in transfer beam. Hence, further exploration is required for the theories and analyses on the seismic performance of the latter structure.

This paper employs the finite-element analysis software OpenSees to promote the seismic performance simulation of frame-supported shear walls. Based on the fibre beam column model (Archbold and Tharmarajah, 2012), the Pinching4 material and zero-length rotational spring were adopted, considering the deformation of longitudinal reinforcement. Then, the seismic numerical analysis model of frame-supported shear wall was established based on reinforcement slip. After that, the author analysed the hysteresis curves and mechanical characteristics against the experiment performed by Chen (Chen et al., 2016), and verified the accuracy of the proposed numerical model.

2. Specimen design

Two specimens were designed for mechanical analysis under cyclic load. One of the specimens was a frame-supported shear wall reinforced with CFRP bars, and the other was reinforced by steel bars and taken as the contrast. The detailed design of the specimens is shown in Figure 1. In the test, the end of CFRP bars did not

Please cite this article as: Yao W., Jiang S., Tao S., Wu S., 2018, Numerical seismic performance model of frame-supported shear wall with carbon fibre reinforced plastic bars in transfer beam based on opensees, Chemical Engineering Transactions, 66, 1117-1122
DOI:10.3303/CET1866187

slip due to the application of anchorage, and the final failure mode of all specimens was bending failure. More details on the experimental design are given in Chen.

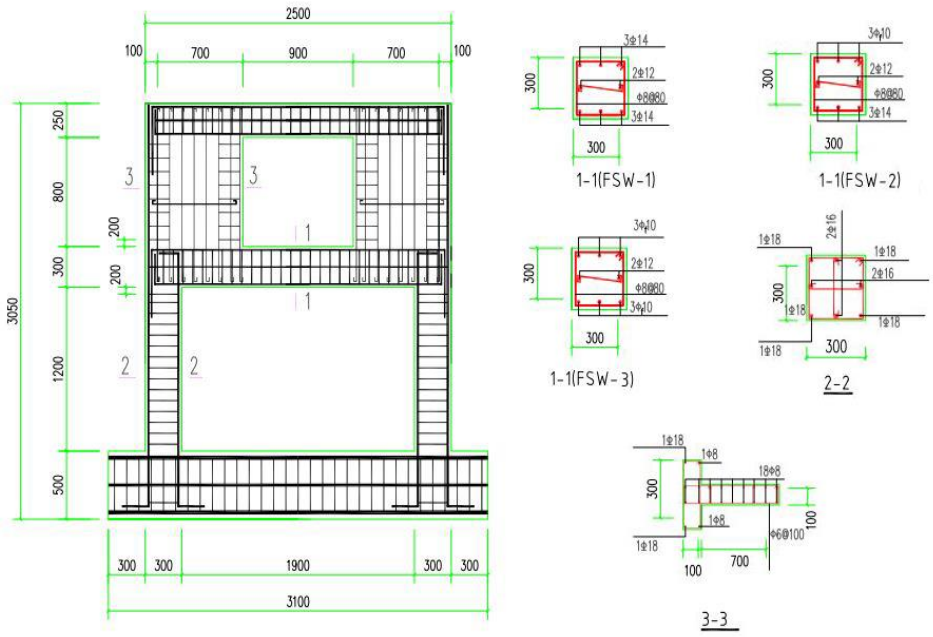

Figure 1: Detailed design of specimens

3. Establishment of analysis model

3.1 Constitutive model of materials

In the cross-section, concrete is restricted by stirrups. Hence, the effect of stirrups should be reasonably reflected in the constitutive relationship of concrete. The constitutive model of concrete is essentially a modified Kent-Park model. In this model, coefficient *k* plays an important role with its excellence reaction to the increase in concrete strength and peak strain resulted from the confinement of stirrups. The coefficient *k* is expressed as follows:

$$k = 1 + \frac{\rho_s f_{vs}}{f_c'} \tag{1}$$

where ρ_s is the stirrup ratio; F_{vs} is the yield strength of stirrups; F'_c is the compressive strength of concrete cylinders.

The Steel02 material in OpenSees was selected as the rebar material, through which the Bauschinger effect and isotropic strain hardening were taken into account under cyclic loading. For the CFRP, the linear elastic material model was adopted.

Under cyclic loading, there is bond slip between rebars and concrete, which greatly affects the stiffness, strength and deformability of structure (Elwood, 2003). In this paper, interface elements (zero-length fibre elements, with Pinching4 material) were adopted to simulate the slip deformation (Mitra and Lowes, 2007). The constitutive model of interface element presenting the bond-slip behaviour was shown in Figure 2. The model mainly consists of three parts, including the multi-linear loading path, the three linear loading/unloading paths, and the three damage response paths. The stiffness and strength degradation of the specimens were examined under cyclic loads. The loading/unloading paths depend on the following parameters: (1) the deformation rate when the maximum/minimum historical deformation is reached under reloading, (2) the loading ratio when the maximum/minimum historical load is reached under reloading; (3) the loading ratio of negative/positive load to the maximum/minimum load path during unloading. In addition, the three damage paths help to simulate the stiffness degradation during unloading, the strength degradation of the previously unreached deformation, and the strength degradation of reloading. The damage index δ is used for each parameter of the three damage paths:

$$\delta_{\mathrm{i}} = \alpha_1 (\tilde{d}_{\max,i})^{\alpha_3} + \alpha_2 (\kappa_i)^{\alpha_4} \le \delta_{\lim} \tag{2}$$

$$\tilde{d}_{\max,i} = \max[\frac{d_{\max,i}}{D_{\max}}, \frac{d_{\min,i}}{D_{\min}}] \tag{3}$$

Where α_i are the parameters determined by the test value; δ_{lim} is the maximum value of damage index; d_{max} and d_{min} are the maximum and minimum values of historical deformation, respectively; D_{max} and D_{min} are the positive and negative deformations at the initial strength damages, respectively; κ is the energy ratio of cumulative hysteresis energy consumed at the maximum deformation under single loading; i is the number of the current loading step.

The stiffness and strength degradations are defined as follows:

$$k_i = k_0 (1 - \delta_{\mathrm{i}}^k) \tag{4}$$

$$f_{\max,i} = f_{\max,0} (1 - \delta_{\mathrm{i}}^f) \tag{5}$$

$$d_{\max,i} = d_{\max,0} (1 - \delta_{\mathrm{i}}^d) \tag{6}$$

Where k_i is the unloading stiffness; δ^k is the damage index of unloading stiffness; f_{max} is the maximum strength in the damage response path; δ^f is the loss index of the strength; d_{max} is the maximum deformation in the previous step during reloading; δ^d is the damage index of deformation; i is the number of current load step.

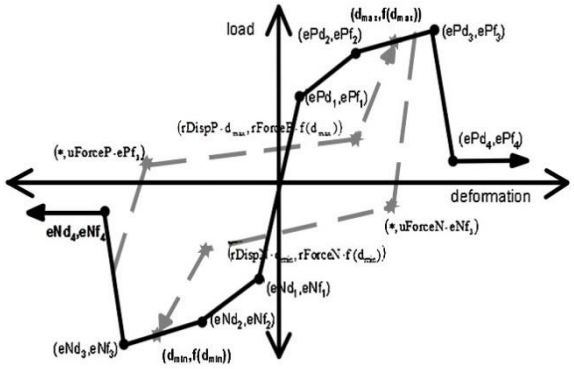

Figure 2: Stress-strain relationship of Pinching4 material model

3.2 Element type and model establishment

OpenSees provides three macro elements of beam columns: Displacement-Based Beam-Column Element, Nonlinear Beam Column Element and Beam With Hinges Element. The first element was adopted for the simulation of frame-supported shear wall structure with CFRP bars.

As the requirements of fibre model, the cross-section must be meshed, allowing the variation of the section stiffness along the length of the rod. The meshing process is explained as follows. First, the elements were divided into several sections by Displacement-Based Beam-Column Element; then, the end displacement of the corresponding element was calculated according to the integral of nodal displacement; next, the section deformation was obtained by Hermite polynomial interpolating function; the resistance vector and tangent stiffness matrix of the corresponding section were derived based on the restoring-force relation of cross-section; finally, the force vector and the stiffness matrix of the entire element along the length of the rod were acquired by the Gauss-Lobatto quadrature rules.

Based solely on material nonlinearity, the stiffness matrix of Displacement-Based Beam-Column Element can be expressed as:

$$[\mathrm{K}]^e = \int_l [B(x)]^T [k(x)]^s [B(x)] dx \tag{7}$$

where [B(x)] is interpolating function of element displacement; $[k(x)]^s$ is the tangent stiffness matrix of the section. Then, the element resistance vector can be expressed as:

$$[Q]^e = \int_l [B(x)]^T [D_R(x)]^s [B(x)] dx \tag{8}$$

Where $[B(x)]$ is interpolating function of element displacement; $[D_R(x)]^s$ is the cross-section resistance matrix.
The beam and column members are properly subdivided in the modelling process, aiming to speed up the computation and reduce the iteration error of the interpolating function. The plastic hinge length is defined as the section height. Since the unit length of fibre element must be shorter than the length of plastic hinge, the transfer beam and column members were divided into five sections. Moreover, the length of the end elements was taken as the section height of element and the middle elements were equally divided.
In view of the bond slip effect of longitudinal reinforcement, a zero-length rotational spring was added to the bottom of the column. In addition, Pinching4 material was given to the zero-length element. The element, also based on the fibre section model, shared the same cross-section dimensions and division method with nonlinear beam column element. The only difference lies in the material: the reinforced constitutive model of the former adopts Pinching4 material, while the latter uses Steel02. In the zero-length rotational spring element, the force-deformation relationship was replaced by the moment-curvature relationship of the section.
During the OpenSees modelling, the zero-length spring element had two nodes of the same coordinates. For deformation calculation, the actual length of element was set to zero, but the sectional length was set to one. Because the element only contained one Gaussian integral point, the deformation (curvature) of a section equalled the element deformation (corner). Therefore, the bond slip deformation of the element can be obtained by the curvature of the zero-length spring element.

4. Results and discussion

4.1 Hysteresis curves

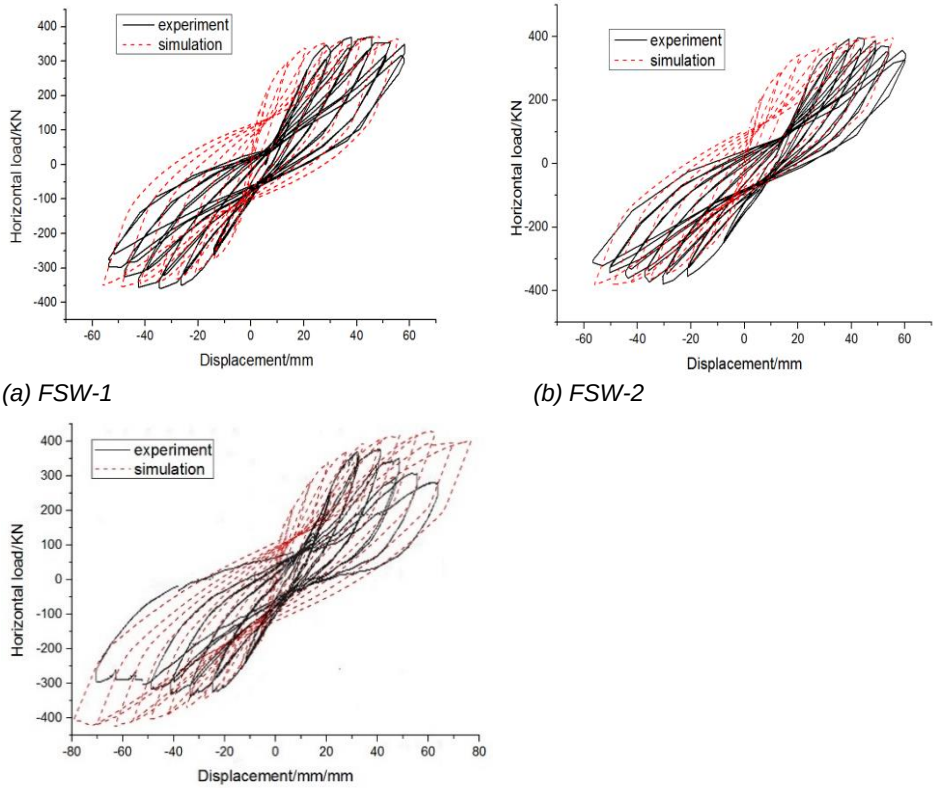

(a) FSW-1 *(b) FSW-2*

(c) FSW-3

Figure 3: Comparison between the experimental and simulated hysteretic curves

As shown in the Figure 3, the hysteresis curves simulated by the model are in good agreement with the experimental results. Overall, the numerical model considering the bond slip does well in simulating the “pinching” phenomenon of hysteretic curves and stiffness degradation features under cyclic load.

In the initial stage of loading, the relationship between horizontal load and displacement changed linearly due to the elastic mode. With the increase in the load, the specimen stiffness of loading and unloading gradually declined, and inflection points appeared on the hysteresis loop. The slope of the restoring force curve demonstrates an initially small but later prominent stiffness on the positive and negative curves. Nevertheless, the unloading curve exhibited an opposite trend. Taking the unloading as an example, lower longitudinal reinforcement in transfer beam had entered the stage of tension yield in the previous positive loading process; when the positive displacement was unloaded, the elastic part of the lower longitudinal reinforcement recovered immediately, but the plastic elongation did not. During unloading, the concrete did not withstand compression because of the original cracks. Then, the reinforcement bars were the only members to bear compression on the lower part of the beam. That is why the cross-section stiffness was small and the curve was gentle. With the further increase of the reverse load, the lower steel bars were pressed to the compressive yield, which closed the original cracks and put the concrete under compression. Hence, the section stiffness entered into the rising path.

4.2 Skeleton curves

The skeleton curves of the specimens were obtained based on the restoring force curves of horizontal load and displacement, which are also reasonably predicted by OpenSees. As shown in Figure 4, the specimens underwent five stages, namely, the elastic stage, the yield stage, the enhancement stage, the ultimate load stage, and the load drop stage. The trend of the skeleton curves was similar to that of the specimens under single loading. With the increase in loading displacement, the specimens surpassed the elastic limit and entered into the yield state. Then, the stress remained constant despite the rapid increase of displacement. As the displacement continued to increase, the bearing capacity of the specimens also rose up.

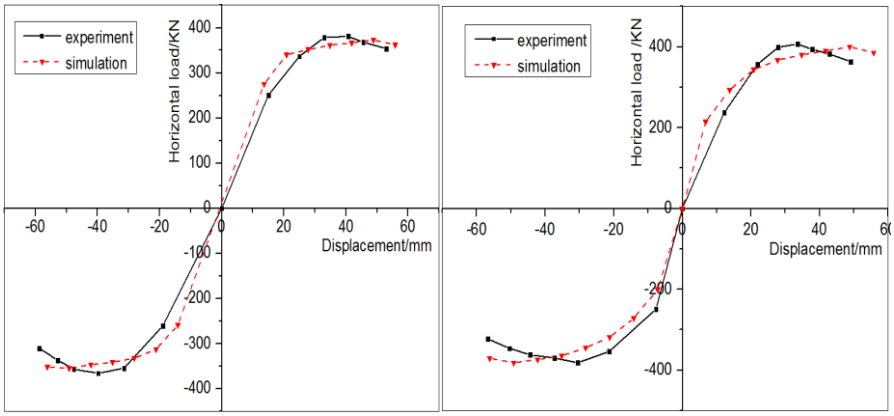

(a) FSW-1 (b) FSW-2

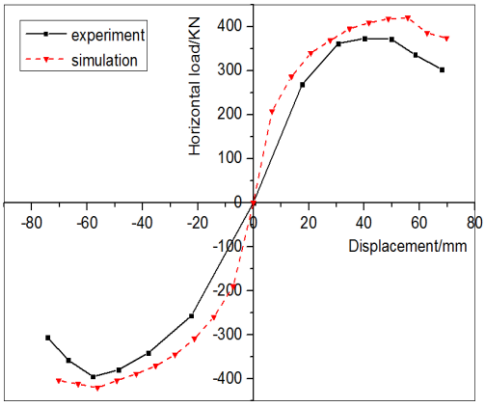

(c) FSW-3

Figure 4: Comparison of skeleton curves

4.3 Analysis of bearing capacity

Table 1 compares the yield load and ultimate load of the specimens obtained by the experiment and the simulation. It can be seen that the structure reinforced by steel bears had the same bearing capacity with the

structure reinforced by CFRP bars. The yield load of each specimen was higher than the experimental value, with an error of about 10%. The error is resulted from the overlook of concrete stiffness degradation after cracking in the OpenSees model.
For FSW-1 and FSW-2, the experiment and simulation agreed well on the ultimate bearing capacity of the specimens; for FSW-3, there was a relatively large difference between the simulated and experimental ultimate bearing capacity, but the overall error was within 12%. The results indicate that our model can accurately describe the mechanical features of the specimens under cyclic loading.

Table 1: Comparison of yield load and ultimate load

specimens	Yield load (kN)			Ultimate load (kN)		
	Test values	Simulate values	Differences (%)	Test values	Simulate values	Differences (%)
FSW-1	265	296.07	11.70	381	373.11	2.07
FSW-2	260	288.74	11.05	394	391.16	0.72
FSW-3	290	319.28	10.10	366.5	410.36	11.97

5. Conclusions

This paper carries out simulation and analysis of the seismic performance of two specimens on frame-supported shear walls, respectively reinforced by steel bars and CFRP bars. Based on the finite-element software OpenSees, a numerical analysis model was established in consideration of the bending deformation and bond slip of longitudinal reinforcement. Then, the simulated hysteresis curves and skeleton curves simulated were contrasted with the test results. The main conclusions are as follows:
(1) The simulated hysteretic curves and bearing capacity of the specimens were consistent with the experimental results, which verified the accuracy of the numerical model.
(2) According to the simulated and experimental results, the frame-supported shear wall reinforced by CFRP bars had a similar bearing capacity with that reinforced by steel bars.

Acknowledgments

The authors are deeply grateful for the finical support from the Key Projects of College Outstanding Achievements Transformation (KJZH14220).

References

Archbold P., Tharmarajah G., 2012, Nonlinear Finite Element Analysis of FRP Reinforced Concrete Structures, In Bridge Research in Ireland and Concrete Research in Ireland Joint Symposium.
Chen J., Jiang S., Zeng X., Sun T., Zhou L., Yao K., 2016, Study on seismic performance of frame-supported shearwall structure partially configured by FRP bars, Journal of building materials, 19(2), 317-324, DOI: 10.3969/j.issn.1007-9629.2016.02.018
Dong Z.H., Han Q., Du X.L., Zhang D.J., 2013, Experimental Study on Seismic Performance of CFRP Confined RC Rectangular Hollow Section Bridge Piers, In China-Japan-Us Trilateral Symposium on Lifeline Earthquake Engineering, 457-464, DOI: 10.1061/9780784413234.059
Elwood K., 2003, PhD Thesis, Shake table tests and analytical studies on the gravity load collapse of reinforced concrete frames, University of California, Berkeley.
Ge, W.J., Zhang J.W., Dai H., Tu Y.M., 2011, Experimental Study on the Flexural Behavior of Concrete Beam Hybrid Reinforced with FRP Bars and Steel Bars, Springer, 301-303, DOI: 10.1007/978-3-642-17487-2_65
Grace N.F., Singh S.B., Shinouda M.M., Mathew S.S., 2005, Concrete Beams Prestressed with CFRP, Concrete International, 27(2), 60-64.
Liang W.S., Cai J., 2011, Nonlinear Static Analysis of Seismic Response for Transfer Structure with Haunching Braces, Advanced Materials Research, 493-498, DOI: 10.4028/www.scientific.net/AMR.255-260.493
Micelli F., Mazzotta R., Leone M., Aiello M.A., 2014, Review Study on the Durability of FRP-Confined Concrete, Journal of Composites for Construction, 19(3), 04014056, DOI: 10.1061/(ASCE)CC.1943-5614.0000520
Mitra N., Lowes L.N., 2007, Evaluation, calibration, and verification of a reinforced concrete beam–column joint model, Journal of Structural Engineering, 133(1), 105-120, DOI: 10.1061/(ASCE)0733-9445(2007)133:1(105)
Whitehead P.A., 2005, Novel Shear Reinforcement for Fiber-Reinforced Polymer-Reinforced and Prestressed Concrete, ACI Structural Journal, 102(2), 286-294.